HHS Public Access

Author manuscript

Clin Exp Metastasis. Author manuscript; available in PMC 2017 April 01.

Published in final edited form as:

Clin Exp Metastasis. 2016 April ; 33(4): 373–383. doi:10.1007/s10585-016-9784-z.

Characterization of passive permeability at the blood-tumor barrier in five preclinical models of brain metastases of breast cancer

Chris E. Adkins[1,2], **Afroz S. Mohammad**[1,2], **Tori Terrell-Hall**[1,2], **Emma L. Dolan**[1], **Neal Shah**[1], **Emily Sechrest**[1], **Jessica Griffith**[1], and **Paul R. Lockman**[1,2,‡]

[1] West Virginia University, Health Sciences Center, School of Pharmacy, Department of Basic Pharmaceutical Sciences, Morgantown, WV 26506, USA

[2] Texas Tech University Health Sciences Center, School of Pharmacy, Department of Pharmaceutical Sciences, Amarillo, TX 79106, USA

Abstract

The blood brain barrier (BBB) is compromised in brain metastases, allowing for enhanced drug permeation into brain. The extent and heterogeneity of BBB permeability in metastatic lesions is important when considering the administration of chemotherapeutics. Since permeability characteristics have been described in limited experimental models of brain metastases, we sought to define these changes in five brain-tropic breast cancer cell lines: MDA-MB-231BR (triple negative), MDA-MB-231BR-HER2, JIMT-1-BR3, 4T1-BR5 (murine), and SUM190 (inflammatory HER2 expressing). Permeability was assessed using quantitative autoradiography and fluorescence microscopy by co-administration of the tracers ^{14}C-aminoisobutyric acid (AIB) and Texas Red conjugated dextran (TRD) prior to euthanasia. Each experimental brain metastases model produced variably increased permeability to both tracers; additionally, the magnitude of heterogeneity was different among each model with the highest ranges observed in the SUM190 (up to 45-fold increase in AIB) and MDA-MB-231BR-HER2 (up to 33-fold in AIB) models while the lowest range was observed in the JIMT-1-BR3 (up to 5.5-fold in AIB) model. There was no strong correlation observed between lesion size and permeability in any of these preclinical models of brain metastases. Interestingly, the experimental models resulting in smaller mean metastases size resulted in shorter median survival while models producing larger lesions had longer median survival. These findings strengthen the evidence of heterogeneity in brain metastases of breast cancer by utilizing five unique experimental models and simultaneously emphasize the challenges of chemotherapeutic approaches to treat brain metastases.

‡**Corresponding Author**: Paul R. Lockman, BSN, Ph.D., Department of Basic Pharmaceutical Sciences, West Virginia University Health Sciences Center, 1 Medical Center Drive, Morgantown, West Virginia, 26506-9050, Phone: 304-293-0944, prlockman@hsc.wvu.edu.
Chris E. Adkins: ciadkins@hsc.wvu.edu
Afroz S. Mohammad: asmohammad@mix.wvu.edu
Neal Shah: nlshah@mix.wvu.edu
Tori Terrell-Hall: tbterrell@mix.wvu.edu
Emma L. Dolan: eldolan@mix.wvu.edu
Emily Sechrest: ersechrest@mix.wvu.edu
Jessica Griffith: jgriff30@mix.wvu.edu

Keywords

blood-brain barrier; blood-tumor barrier; brain metastasis; breast cancer; permeability

Introduction

Effective drug delivery to brain metastases relies on a chemotherapeutic's ability to penetrate the blood-brain barrier (BBB) and/or blood-tumor barrier (BTB) such that adequate concentrations of therapeutics accumulate within lesions [1]. Despite the constant development of promising new drugs to treat primary breast cancer [2], fewer than 2% of new central nervous system (CNS) drug candidates receive approval for clinical use because of suboptimal BBB penetration [3]. The BBB employs both morphologic and physiologic characteristics that distinguish brain vasculature from peripheral vasculature [4]. The presence of these physical, enzymatic, and transport barriers of the BBB collectively serves a protective and regulatory role by preventing potentially deleterious compounds and substances from gaining access to the CNS [5,6].

The capillary endothelial cells that contribute to the BBB are structurally reinforced by a dense network of tight junction proteins that restrict drug distribution into brain by forming a physical barrier that limits drug diffusion from blood to brain [7,8]. These tight junction proteins anchor capillary endothelial cells together such that the transendothelial electrical resistance (TEER) across brain capillary endothelial cells is significantly greater than peripheral vascular endothelial cells [9,10]. Essentially, tight junction proteins at the BBB reinforce the intercellular interface between capillary endothelial cells similar to a continuous cell membrane. Further, the close association of pericytes and astrocyte foot processes surrounding the vascular endothelial cells of the BBB provide additional physical barriers, which limit passive diffusion of polar and large drugs into brain [11-13]. In addition to the physical barriers presented by the vascular endothelium, pericytes, and astrocyte foot processes, these cells express a number of drug metabolizing enzymes that inactivate drugs that can further reduce the distribution of active drugs to brain [14,15]. Overall, the passive diffusion of most drugs, particularly those having a large molecular weight, are charged, and hydrophilic show limited permeation into brain compared to drugs that are small, uncharged, and lipophilic [16-18].

The growth of metastases within the brain has been shown to variably contribute to increased permeability of the adjacent neurovasculature [19,20]. Cells supporting the neurovasculature, such as pericytes and astrocytes, lose intimate association with capillary endothelial cells during the proliferation of intracranial metastases, which compromise the integrity of the BBB resulting in increased permeability [21-23]. Brain microvessels associated with proliferating metastases develop fenestrations [24], increase pinocytic vesicles [25], and exhibit decreased and displaced tight junction proteins [26,27]. The permeability of the microvasculature of brain tumors and metastatic lesions (blood-tumor barrier; BTB) has been reported to range from one to two orders of magnitude greater than normal brain vasculature [28,29]. The increases in BTB permeability makes magnetic resonance imaging (MRI) of metastatic lesions possible by enhancing gadolinium

permeation across tumor microvessels [30]. Importantly, drug distribution and, to a certain degree, efficacy of chemotherapy has been shown to correlate with BTB permeability [31,32]. Therefore, the evaluation of vascular permeability in experimental brain metastases models will provide insight into clinical responses to chemotherapy and may help to inform the design of novel chemotherapeutics that must penetrate the BTB to achieve efficacy.

Herein, we have characterized BTB permeability using two passive permeability markers, ^{14}C-AIB (104 Da) and Texas Red dextran (TRD)(3kDa), in five experimental models of brain metastases of breast cancer in mice. These brain-tropic cell lines include the MDA-MB 231BR and the MDA-MB-231BR-HER2+ line (a HER-2 transfectant of the MDA-MB-231BR [33]). We also evaluate a recently reported naturally overexpressing HER2+ cell line (JIMT-1-BR3) [34], the 4T1-BR5 [35], a brain seeking line derived from the murine 4T1 mammary carcinoma cell line, and lastly the estrogen receptor negative/ HER2+ SUM190 inflammatory breast cancer cell line that is also brain specific (denoted as SUM190-BR3). We observed that all metastases from each cell line demonstrated a significant increase in permeability compared to normal brain with both passive markers. Passive permeability increases were highest in the SUM190-BR3 (for ^{14}C-AIB) and 4T1-BR5 (for TRD) model and lowest in the JIMT-1-BR3 (for ^{14}C-AIB) and MDA-MB-231BR (for TRD) model. Further, permeability changes varied both within and in between metastases without an apparent pathological correlation to size, density or invasiveness. Lastly, relevant to the model used predominantly in this experiment, we observed that changes in BTB permeability in the MDA-MB-231BR cell line significantly increased during the period of 21-28 days of development and stayed relatively stable until death.

Materials & Methods

Chemicals & Reagents

Texas Red conjugated dextran (3kDa) (TRD) was purchased from Molecular Probes-Life Technologies (Carlsbad, CA).^{14}C-labelled aminoisobutyric acid (AIB) was purchased from American Radiolabelled Chemicals (St. Louis, MO). Cresyl violet acetate (0.1%) was purchased from Sigma-Aldrich (St. Louis, MO). Firefly D-luciferase potassium salt was purchased from Caliper-PerkinElmer (Waltham, MA). All chemicals and reagents used were of analytical grade and were used as supplied.

Cell culture

Human MDA-MB-231BR, JIMT-1-BR3, and murine 4T1-BR5 mammary carcinoma cells were grown in DMEM supplemented with 10% FBS. Human MDA-MB-231-HER2+ metastatic breast cancer cells over-expressing HER2 (also expressing enhanced green fluorescent protein, eGFP) were cultured in DMEM supplemented with 10% FBS and Zeocin (300 μg/mL). SUM190-BR3 cells were grown in Ham-F12 media supplemented with 1 μg/ml hydrocortisone, 10 mM HEPES, 5 μg/ml insulin, 50 nM sodium selenite, 5 μg/ml transferrin, 10 nM tri-iodothyronine (T3), and 1 g/L bovine serum albumin (BSA). All cells were used in passages 1-10 and maintained at 37°C with 5% CO2. For all cell preparations for intracardiac injection, cells were harvested at 70% confluency. All cell lines were kindly provided by the laboratory of Dr. Patricia Steeg at the National Cancer Institute.

Experimental brain metastases model

Experiments were conducted under approved institutional Animal Care and Use Committee protocols (TTUHSC #06024 and WVU #13-1207) and all work followed internationally recognized animal welfare guidelines. Female athymic nu/nu mice (24-30 g) were purchased from Charles River Laboratories (Wilmington, MA) and were used as the experimental metastases platform in this study. All animals were 6 to 8 weeks of age at the initiation of the metastases models and were housed in a barrier facility. Mice were anesthetized under 2% isoflurane and inoculated with 175,000 breast cancer cells (for each model) in the left cardiac ventricle with the aid of a stereotaxic device (Stoelting, Wood Dale, IL). Injection accuracy was evaluated by a pulsatory flow of bright red blood into the syringe upon slight retraction of the plunger prior to injection. After intracardiac injection, mice were placed in a warmed (37°C) sterile cage and vitals monitored until fully recovered. Metastases were allowed to develop until neurologic symptoms appeared (12 – 70 days) and animals were anesthetized with ketamine/xylazine (100mg/kg and 8mg/kg respectively) prior to TRD (6mg/kg) and ^{14}C-AIB (10 or 25μCi) injection via IV bolus dose (femoral vein). The TRD and ^{14}C-AIB were allowed to circulate for 10 minutes prior to euthanasia. Immediately, the brain was rapidly removed (less than 60 seconds) and flash-frozen in isopentane (−65°C) and stored at negative 20°C.

Tissue processing and analysis

Brain slices (20μm thick) were acquired with a cryotome (Leica CM3050S; Leica Microsystems, Wetzlar, Germany) and transferred to charged microscope slides (3 brain slices per microscope slide; each brain produces approximately 70-100 slides total). Fluorescence images of brain slices were acquired using a stereomicroscope (Olympus MVX10; Olympus, Center Valley, PA) equipped with a 0.5 NA 2X objective and a monochromatic cooled CCD scientific camera (Retiga 4000R, QIMaging, Surrey, BC, Canada). Texas Red fluorescence was imaged using a DsRed sputter filter (excitation/band λ 545/25nm, emission/band λ 605/70nm and dichromatic mirror at λ 565nm) (Chroma Technologies, Bellows Falls, VT) and enhanced green fluorescent protein (expressed in MDA-MB-231BR-HER2+) using an ET-GFP sputter filter (excitation/band λ 470/40nm, emission/band λ 525/50nm and dichromatic mirror at λ 495nm) (Chroma Technologies, Bellows Falls, VT). Fluorescence image capture and analysis software (SlideBook 5.0; Intelligent Imaging Innovations Inc., Denver, CO) was used to capture and quantitate fluorescence images. Texas Red permeability fold-changes were determined by Texas Red sum intensity (SI) per unit area of metastases relative to the SI per area of contralateral normal brain regions. If metastases occurred in contralateral regions, adjacent slices containing unaffected tissues of the same brain structure were used as comparative normal brain regions.

Quantitative autoradiography (QAR)

After fluorescence imaging of tissue, slides were placed in QAR cassettes (FujiFilm Life Sciences, Stamford, CT) along with ^{14}C autoradiographic standards (GE Healthcare, Piscataway, NJ). A phosphor screen (FujiFilm Life Sciences, 20 × 40 super-resolution) was placed with the slides and standards and allowed to develop for 6 up to 14 days. QAR

phosphor screens were developed in a high-resolution phosphor-imager (FUJI FLA-7000, FujiFilm Life Sciences) and converted to digital images. Digital QAR images were calibrated to ^{14}C standards and analyzed using MCID Analysis software (InterFocus Imaging LTD, Linton, Cambridge, England). Metastases permeability fold-changes were calculated based on ^{14}C-AIB signal intensity within confirmed metastases locations (determined by cresyl violet or eGFP fluorescence image overlays) relative to contralateral normal brain ^{14}C-AIB signal intensity.

Cresyl Violet Staining

Tissue sections were processed as described above and subsequently fixed using 4% paraformaldehyde followed by a rinse in PBS for 10 minutes. Staining was performed using 0.1% cresyl violet acetate (Sigma-Aldrich, St. Louis, MO) (15 minutes) followed by rinsing in H_20. Sections were cleared in 70% ethanol (15 seconds), 95% ethanol (30 seconds), 100% ethanol (30 seconds), respectively. Images were obtained with a 2x objective on an inverted microscope (Olympus IX81) equipped with a color camera (Olympus DP71).

Statistics

XY plots were analyzed by linear regression (GraphPad Prism software). Median and interquartile range (IQR) values are used for tumor permeability fold changes and metastasis size because these did not belong to a Gaussian population (D'Agostino & Pearson omnibus normality test). Box and whisker plots represent median and interquartile ranges (IQR) with 5-95% percentile whiskers; statistical analysis done with Kruskal-Wallis followed by Dunn's multiple comparison test (*$p<0.05$, **$p<0.01$). Animal median survival data was analyzed using the log-rank test.

Results

In our first set of experiments we characterized BTB permeability (Fig. 1) of 4T1 metastases (n=229), which developed approximately 14 days after inoculating cells into the left cardiac ventricle. We characterized the 4T1 cell line since it is a highly metastatic cell line and can colonize in the lungs, liver, bone, and brain [35]. This model is often used to study the role of the immune system in tumor growth and metastasis since it is syngeneic in BALB/c mice [36]. We observed that when the animals developed neurological symptoms, passive permeability changes in the metastatic lesion ranged from 0.7 to 13-fold over normal brain with a median (IQR) fold change of 3.02 (2.2-4.5) for ^{14}C-AIB (Fig. 1a). For the passive diffusion marker Texas Red dextran (TRD), permeability ranged from 0.9 to 7.6-fold with a median (IQR) fold change of 2.53 (2.0-3.1) (Fig. 1b). There was a poor correlation (r^2= 0.23) to changes in ^{14}C-AIB passive permeability and size of the lesion (Fig. 1a). No correlation was observed (r^2=0.07) for TRD passive permeability and metastasis size (Fig. 1b).

The next model we evaluated was a brain-tropic derivative of the epithelial human carcinoma cell line JIMT-1 [34]. The primary cell line was established from a pleural metastasis of a 62-year-old breast cancer patient. This cell line has a naturally overexpressing HER-2 oncogene, which overproduces both HER-2 mRNA and the protein.

Parent JIMT-1 cells do not express estrogen or progesterone receptors. Of interest, JIMT-1 cells are insensitive to trastuzumab and pertuzumab [34]. Passive permeability changes in the JIMT-1-BR3 metastatic lesions (n=256) at the time when brain metastases began to produce neurological symptoms were less than that of the 4T1 model, ranging from 1.1 to ~6-fold over normal brain with a median (IRQ) fold change of 2.08 (1.8-2.5) for ^{14}C-AIB (Fig. 2a). Passive permeability of TRD fold changes ranged from 0.8 to 2.7-fold with a median (IQR) of 1.43 (1.3-1.6) (Fig. 2b). As seen with the previous model, no correlation (r^2=0.004 for ^{14}C-AIB and r^2=0.007 for TRD) (Fig. 2a & 2b) between passive permeability and lesion size was observed.

Given that the JIMT-1 line is a naturally overexpressing HER2 cell line, we also chose to evaluate the brain-tropic MDA-MB-231BR-HER2+ cell line transfected to overexpress HER2. The parent MDA-MB-231 cell line is a triple negative human cell line (estrogen, progesterone and HER2 receptor negative) that was derived from a metastatic adenocarcinoma of the mammary gland of a 51-year-old Caucasian woman and is epithelial in nature but poorly differentiated [37]. The parent line is highly aggressive and invasive, which has been useful in experimental metastases models studying various tissues [38]. Unlike the JIMT-1-BR3, line the MDA-MB-231BR-HER2+ model produced metastatic lesions (n=137) with higher permeability relative to normal brain for both ^{14}C-AIB and TRD (Fig. 3). Passive permeability fold changes ranged from 0.95 to 34-fold with a median (IQR) of 5.51 (3.1-8.8) for ^{14}C-AIB (Fig. 3a) while TRD permeability fold changes (Fig. 3b) ranged from 0.91 to 8.4-fold with a median (IQR) of 1.18 (1.1-1.6). However, similar to the previous models, we observed no correlation between passive permeability and tumor size (r^2=0.03 for ^{14}C-AIB and r^2=0.06 for TRD) (Fig. 3a & 3b) in the MDA-MB-231BR-HER2 model.

Since we did not see an initial correlation between HER2 and increases in lesion permeability, we then evaluated permeability in the brain seeking MDA-MB-231BR cell line model (without the HER2 transfectant). In this model we observed lesion (n=235) permeability changes (Fig. 4a & 4b) when the animals developed neurological symptoms that were greater than the 4T1 and JIMT1 cell line model, but less than the MDA-MB-231BR-HER2+ transfected model. Specifically, MDA-MB-231BR permeability changes with ^{14}C-AIB (Fig. 4a) ranged 0.79 to 19-fold above normal brain with a median (IQR) of 2.31 (1.6-3.6). The BTB permeability to TRD (Fig. 4b) ranged from 0.78 to 4.0-fold with a median (IQR) of 1.1 (1.0-1.2). Similar to the HER2 transfected line, there was no correlation between passive permeability and size (r^2=0.08, ^{14}C-AIB; r^2=0.03, TRD) (Fig. 4a & 4b).

The SUM190 cell line is a poorly differentiated inflammatory breast carcinoma. It does not express progesterone or estrogen receptors, but does express HER2 receptors [39]. Of note, inflammatory breast cancer tumors grow quickly and invade rapidly, and are typically highly vascular due to increased VEGF secretion [40], so we hypothesized permeability could be compromised in brain metastases. The experimental SUM190-BR3 model produced metastatic lesions with the greatest permeability, and variability, relative to normal brain for ^{14}C-AIB (Fig. 5a); permeability fold changes ranged from 0.99 to 49-fold and had a median (IQR) of 11.9 (7.7-16.3). Although the ^{14}C-AIB in this model was greater relative to

the other models tested, TRD permeability (Fig. 3b) remained modest exhibiting only a 0.74 to 3.5-fold increase and a median (IQR) of 1.43 (1.2-1.7). Like each of the previous models, the correlation of ^{14}C-AIB permeability and metastasis size in the SUM190-BR3 cell line (n=285 metastases) was poor (r^2=0.21; Fig. 5a) and the Texas Red dextran (n=143 metastases analyzed) permeability showed no correlation (r^2=0.008; Fig. 5b) to lesion size.

Following the evaluation of permeability in each model, we compared the size of metastatic lesions in brain once animals became moribund (Fig 6a). Finally, we assessed the median survival in each model of experimental brain metastases of breast cancer (Fig 6b). The shortest median survival occurred in the 4T1-BR5 syngeneic model (14 days) while the highest median survival was seen in the SUM190-BR3 model (92 days). Of interest, median survival corresponded with the rank order of metastasis size, i.e., the longer the animal survived the larger the lesions. For example, the median survival time with the 4T1-BR5 cell line was 14 days and the resulting median (IQR) tumor size was 0.30 (0.12-0.40) mm^2 while the SUM190-BR3 cell line exhibited a median survival time of 92 days with corresponding median (IQR) tumor size of 0.66 (0.31-1.5) mm^2. Overall, we analyzed passive permeability in 998 experimental brain metastases in five different models. Permeability fold change values and their correlation to metastasis size are summarized in Table 1.

Discussion

Herein we have characterized five breast cancer cell lines in an experimental model of metastases, which preferentially seed the brain. We have demonstrated that there are differences in the magnitude of passive permeability changes between each experimental model of brain metastases. Not surprisingly, we observed differences in median survival and the size of metastatic lesions at the time animals became moribund. The increased permeability of the vasculature at the BTB is critically important for both diagnosis and treatment. Imaging contrast agents such as gadolinium gain access to the CNS through increased vascular permeability within CNS lesion and are, therefore, useful in the clinic to define tumor location, the amount of peri-tumoral edema, vascularity of the lesion, and potentially the tumor type [41]. Recently, surgical oncologists have utilized the enhanced uptake of contrast agents such as gadolinium into CNS lesions as a guide during tumor resection as well as a tool to estimate patient prognosis and response to therapy [42]. Of interest to our work, some CNS tumor types appear non-enhancing or low enhancing in magnetic resonance imaging [43,44], which suggests that vascular permeability changes in some tumor types are less than pronounced than other tumor types. Further, metastatic lesions have varying degrees of enhancement depending on type of tumor and location [45]. Our permeability work (notably with the small marker AIB) agrees with clinical imaging data suggesting not all lesions demonstrate enhancement to contrast agents uniformly.

Consistent with previous work [31,46], we demonstrate that changes in passive permeability are independent of lesion size, and do not appear to be related to tumor morphology. Moreover, the observed BTB permeability at different locations within the brain did not appear to influence permeability in these models supporting previous MRI studies examining the distribution of gadolinium-enhancing metastases in similar preclinical models [19]. The brain distribution of metastatic foci in each model presented herein appear

consistent with similar studies demonstrating more than 50% of metastatic burden occurs in cortical regions, with relatively fewer lesions occurring in the central brain regions, and the least metastatic growth observed in the posterior and olfactory regions [47,48]. Additionally, this work agrees with previous findings [46] suggesting the presence of HER2 does not seem to correlate strongly with changes in vascular permeability (permeability of JIMT-1-BR3, SUM190-BR3, and MDA-MB-231BR-HER2+ lines were not congruent) and that permeability changes appear to be more cell line specific (i.e., MDA-BB-231BR and MDA-MB-231BR-HER2+). Interestingly, Murell et. al. observed much smaller SUM190-BR3 brain metastases relative to MDA-MB-231BR-HER2+. In our hands, the SUM190-BR3 model produced the largest metastases relative to the other four models of experimental brain metastases. This observation may be due to differences in experimental approaches such as the density of cells injected; for instance, Murrell et. al. injected 5×10^5 SUM190-BR3 cells compared to 1.75×10^5 cells used to initiate our model. Similarly, number of cells injected has been previously shown to affect the number of metastases in preclinical brain metastases models [47,49]. Despite the observed differences in relative lesion sizes and the reported sizes of SUM190-BR3 by Murrell et al., we observed similar survival patterns as those reported by their group. Inflammatory breast cancer metastases exhibit similar variability of permeability when compared to non-inflammatory breast cancer metastases, though tumor size and median survival in the SUM190-BR3 model was greater relative to other models characterized herein.

It has been demonstrated that changes in lesion passive permeability are highly correlated to the degree of drug uptake as well as drug effect [31]. Unfortunately, the magnitude of passive permeability changes observed in this work, as well as earlier work [31], suggest that fewer than ~10% of metastatic lesions exhibit a BTB vasculature leaky enough to permit efficacious drug concentrations into metastatic lesions using conventional chemotherapeutics. While the rules that govern CNS drug penetration have been studied extensively, drugs predicted to demonstrate excellent CNS distribution do not always translate to therapeutic concentrations of drug accessing brain parenchyma and metastatic cells within the brain. Various chlorambucil analogs, for example, with LogP values ranging between ~4.0 to 8.0 did not exhibit increased brain distribution than chlorambucil (LogP of ~2.6) due to greater peripheral distribution [50]. Similarly, the lipid soluble chemotherapeutic lapatinib produced drug concentrations in brain metastases only 10-20% of what was observed in peripheral tumors [32]. This continues to highlight the need to develop novel drug formulations that specifically take advantage of this variable increase in BTB permeability to elevate and extend drug exposure within intracranial metastases. The integration of PEGylation as polymeric anti-cancer formulations, for example, has been shown to extend the plasma half-life of active drug equivalents without increasing toxicity and facilitate distribution to brain tumors by taking advantage of enhanced permeability at the BTB [51].

Still, we do not fully understand what causes the variability in permeability changes among lesions of the same cell line within the same brain. It has been suggested that increased permeability may be related to any combination of the following factors: breakdown of the astrocyte-vascular endothelial interaction and loss of vascular pericyte coverage [52], increased eNOS synthesis secondary to VEGF secretion from cancer cells [53], the presence

of inflammatory cytokines such as TGFβ [54], the process of angiogenesis [55], and the dysregulation of tight junction proteins in the BTB [56]. Changes in vascular permeability may actually be a representation of all factors at one given time in the local tumor microenvironment. It is entirely possible that lesions in the CNS are undergoing varying degrees of remodeling, growth, and angiogenesis. Accordingly, we might be observing a single static snapshot of the vascular permeability at the time of sacrifice rather than a longitudinal and dynamic observation. Future work should set out to determine if permeability varies longitudinally as lesions develop, which may help improve clinical outcomes of brain metastases of breast cancer.

Acknowledgements

This research was supported by grants from the National Cancer Institute (R01CA166067-01A1) and National Institute of General Medical Sciences (P30GM103488, and GM103434). Additional support for this research was provided by WVCTSI through the National Institute of General Medical Sciences of the National Institutes of Health under Award Number U54GM104942. A portion of this work was completed at each institution mentioned in the author affiliations.

Abbreviations

BBB	blood brain barrier
BTB	blood-tumor barrier
AIB	aminoisobutyric acid
TRD	Texas Red dextran
CNS	central nervous system
TEER	transendothelial electrical resistance
MRI	magnetic resonance imaging
VEGF	vascular endothelial growth factor
eNOS	endothelial nitric oxide synthase
TGFß	transforming growth factor beta

References

1. Palmieri D, Smith QR, Lockman PR, Bronder J, Gril B, Chambers AF, Weil RJ, Steeg PS. Brain metastases of breast cancer. Breast disease. 2006; 26:139–147. [PubMed: 17473372]
2. Lin NU, Amiri-Kordestani L, Palmieri D, Liewehr DJ, Steeg PS. CNS metastases in breast cancer: old challenge, new frontiers. Clinical cancer research : an official journal of the American Association for Cancer Research. 2013; 19(23):6404–6418. doi:10.1158/1078-0432.CCR-13-0790. [PubMed: 24298071]
3. Pardridge WM. Drug transport across the blood-brain barrier. Journal of cerebral blood flow and metabolism : official journal of the International Society of Cerebral Blood Flow and Metabolism. 2012; 32(11):1959–1972. doi:10.1038/jcbfm.2012.126.
4. Abbott NJ, Patabendige AA, Dolman DE, Yusof SR, Begley DJ. Structure and function of the blood-brain barrier. Neurobiology of disease. 2010; 37(1):13–25. doi:10.1016/j.nbd.2009.07.030. [PubMed: 19664713]

5. Hawkins BT, Davis TP. The blood-brain barrier/neurovascular unit in health and disease. Pharmacological reviews. 2005; 57(2):173–185. doi:57/2/173 [pii] 10.1124/pr.57.2.4. [PubMed: 15914466]
6. Abbott NJ. Blood-brain barrier structure and function and the challenges for CNS drug delivery. Journal of inherited metabolic disease. 2013 doi:10.1007/s10545-013-9608-0.
7. Engelhardt B, Liebner S. Novel insights into the development and maintenance of the blood-brain barrier. Cell Tissue Res. 2014; 355(3):687–699. doi:10.1007/s00441-014-1811-2. [PubMed: 24590145]
8. Luissint AC, Artus C, Glacial F, Ganeshamoorthy K, Couraud PO. Tight junctions at the blood brain barrier: physiological architecture and disease-associated dysregulation. Fluids and barriers of the CNS. 2012; 9(1):23. doi:10.1186/2045-8118-9-23. [PubMed: 23140302]
9. Butt AM, Jones HC, Abbott NJ. Electrical resistance across the blood-brain barrier in anaesthetized rats: a developmental study. J Physiol. 1990; 429:47–62. [PubMed: 2277354]
10. Santaguida S, Janigro D, Hossain M, Oby E, Rapp E, Cucullo L. Side by side comparison between dynamic versus static models of blood-brain barrier in vitro: a permeability study. Brain research. 2006; 1109(1):1–13. doi:10.1016/j.brainres.2006.06.027. [PubMed: 16857178]
11. Abbott NJ, Khan EU, Rollinson CM, Reichel A, Janigro D, Dombrowski SM, Dobbie MS, Begley DJ. Drug resistance in epilepsy: the role of the blood-brain barrier. Novartis Foundation symposium. 2002; 243:38–47. discussion 47-53, 180-185. [PubMed: 11990780]
12. Geldenhuys WJ, Mohammad AS, Adkins CE, Lockman PR. Molecular determinants of blood-brain barrier permeation. Therapeutic delivery. 2015:1–11. doi:10.4155/tde.15.32. [PubMed: 25565435]
13. Sa-Pereira I, Brites D, Brito MA. Neurovascular unit: a focus on pericytes. Molecular neurobiology. 2012; 45(2):327–347. doi:10.1007/s12035-012-8244-2. [PubMed: 22371274]
14. Dutheil F, Jacob A, Dauchy S, Beaune P, Scherrmann JM, Decleves X, Loriot MA. ABC transporters and cytochromes P450 in the human central nervous system: influence on brain pharmacokinetics and contribution to neurodegenerative disorders. Expert Opin Drug Metab Toxicol. 2010; 6(10):1161–1174. doi:10.1517/17425255.2010.510832. [PubMed: 20843279]
15. Meyer J, Rauh J, Galla HJ. The susceptibility of cerebral endothelial cells to astroglial induction of blood-brain barrier enzymes depends on their proliferative state. Journal of neurochemistry. 1991; 57(6):1971–1977. [PubMed: 1719132]
16. Groothuis DR. The blood-brain and blood-tumor barriers: a review of strategies for increasing drug delivery. Neuro Oncol. 2000; 2(1):45–59. [PubMed: 11302254]
17. Levin VA. Relationship of octanol/water partition coefficient and molecular weight to rat brain capillary permeability. Journal of medicinal chemistry. 1980; 23(6):682–684. [PubMed: 7392035]
18. Banks WA. Characteristics of compounds that cross the blood-brain barrier. BMC neurology 9 Suppl. 2009; 1:S3. doi:10.1186/1471-2377-9-S1-S3.
19. Percy DB, Ribot EJ, Chen Y, McFadden C, Simedrea C, Steeg PS, Chambers AF, Foster PJ. In vivo characterization of changing blood-tumor barrier permeability in a mouse model of breast cancer metastasis: a complementary magnetic resonance imaging approach. Investigative radiology. 2011; 46(11):718–725. doi:10.1097/RLI.0b013e318226c427. [PubMed: 21788908]
20. Price JE, Zhang RD. Studies of human breast cancer metastasis using nude mice. Cancer metastasis reviews. 1990; 8(4):285–297. [PubMed: 2182209]
21. Raza A, Franklin MJ, Dudek AZ. Pericytes and vessel maturation during tumor angiogenesis and metastasis. American journal of hematology. 2010; 85(8):593–598. doi:10.1002/ajh.21745. [PubMed: 20540157]
22. Fidler IJ, Balasubramanian K, Lin Q, Kim SW, Kim SJ. The brain microenvironment and cancer metastasis. Molecules and cells. 2010; 30(2):93–98. doi:10.1007/s10059-010-0133-9. [PubMed: 20799011]
23. Dubois LG, Campanati L, Righy C, D'Andrea-Meira I, Spohr TC, Porto-Carreiro I, Pereira CM, Balca-Silva J, Kahn SA, DosSantos MF, Oliveira Mde A, Ximenes-da-Silva A, Lopes MC, Faveret E, Gasparetto EL, Moura-Neto V. Gliomas and the vascular fragility of the blood brain barrier. Frontiers in cellular neuroscience. 2014; 8:418. doi:10.3389/fncel.2014.00418. [PubMed: 25565956]

24. Shibata S. Ultrastructure of capillary walls in human brain tumors. Acta neuropathologica. 1989; 78(6):561–571. [PubMed: 2554636]
25. Hirano A, Matsui T. Vascular structures in brain tumors. Human pathology. 1975; 6(5):611–621. [PubMed: 1100515]
26. Davies DC. Blood-brain barrier breakdown in septic encephalopathy and brain tumours. Journal of anatomy. 2002; 200(6):639–646. [PubMed: 12162731]
27. Papadopoulos MC, Saadoun S, Binder DK, Manley GT, Krishna S, Verkman AS. Molecular mechanisms of brain tumor edema. Neuroscience. 2004; 129(4):1011–1020. doi:S030645220400418X [pii] 10.1016/j.neuroscience.2004.05.044 [doi]. [PubMed: 15561416]
28. Gerstner ER, Fine RL. Increased permeability of the blood-brain barrier to chemotherapy in metastatic brain tumors: establishing a treatment paradigm. Journal of clinical oncology : official journal of the American Society of Clinical Oncology. 2007; 25(16):2306–2312. doi:25/16/2306 [pii] 10.1200/JCO.2006.10.0677 [doi]. [PubMed: 17538177]
29. Hiesiger EM, Voorhies RM, Basler GA, Lipschutz LE, Posner JB, Shapiro WR. Opening the blood-brain and blood-tumor barriers in experimental rat brain tumors: the effect of intracarotid hyperosmolar mannitol on capillary permeability and blood flow. Annals of neurology. 1986; 19(1):50–59. doi:10.1002/ana.410190110. [PubMed: 3080944]
30. Runge VM, Clanton JA, Price AC, Wehr CJ, Herzer WA, Partain CL, James AE Jr. The use of Gd DTPA as a perfusion agent and marker of blood-brain barrier disruption. Magn Reson Imaging. 1985; 3(1):43–55. [PubMed: 3923292]
31. Lockman PR, Mittapalli RK, Taskar KS, Rudraraju V, Gril B, Bohn KA, Adkins CE, Roberts A, Thorsheim HR, Gaasch JA, Huang S, Palmieri D, Steeg PS, Smith QR. Heterogeneous blood-tumor barrier permeability determines drug efficacy in experimental brain metastases of breast cancer. Clinical cancer research : an official journal of the American Association for Cancer Research. 2010; 16(23):5664–5678. doi:10.1158/1078-0432.CCR-10-1564. [PubMed: 20829328]
32. Taskar KS, Rudraraju V, Mittapalli RK, Samala R, Thorsheim HR, Lockman J, Gril B, Hua E, Palmieri D, Polli JW, Castellino S, Rubin SD, Lockman PR, Steeg PS, Smith QR. Lapatinib distribution in HER2 overexpressing experimental brain metastases of breast cancer. Pharmaceutical research. 2012; 29(3):770–781. doi:10.1007/s11095-011-0601-8. [PubMed: 22011930]
33. Palmieri D, Bronder JL, Herring JM, Yoneda T, Weil RJ, Stark AM, Kurek R, Vega-Valle E, Feigenbaum L, Halverson D, Vortmeyer AO, Steinberg SM, Aldape K, Steeg PS. Her-2 overexpression increases the metastatic outgrowth of breast cancer cells in the brain. Cancer research. 2007; 67(9):4190–4198. doi:10.1158/0008-5472.CAN-06-3316. [PubMed: 17483330]
34. Tanner M, Kapanen AI, Junttila T, Raheem O, Grenman S, Elo J, Elenius K, Isola J. Characterization of a novel cell line established from a patient with Herceptin-resistant breast cancer. Molecular cancer therapeutics. 2004; 3(12):1585–1592. [PubMed: 15634652]
35. Tao K, Fang M, Alroy J, Sahagian GG. Imagable 4T1 model for the study of late stage breast cancer. BMC cancer. 2008; 8:228. doi:10.1186/1471-2407-8-228. [PubMed: 18691423]
36. Heppner GH, Miller FR, Shekhar PM. Nontransgenic models of breast cancer. Breast cancer research : BCR. 2000; 2(5):331–334. [PubMed: 11250725]
37. Cailleau R, Young R, Olive M, Reeves WJ Jr. Breast tumor cell lines from pleural effusions. J Natl Cancer Inst. 1974; 53(3):661–674. [PubMed: 4412247]
38. Guise TA, Yin JJ, Taylor SD, Kumagai Y, Dallas M, Boyce BF, Yoneda T, Mundy GR. Evidence for a causal role of parathyroid hormone-related protein in the pathogenesis of human breast cancer-mediated osteolysis. The Journal of clinical investigation. 1996; 98(7):1544–1549. doi: 10.1172/JCI118947. [PubMed: 8833902]
39. Grigoriadis A, Mackay A, Noel E, Wu PJ, Natrajan R, Frankum J, Reis-Filho JS, Tutt A. Molecular characterisation of cell line models for triple-negative breast cancers. BMC Genomics. 2012; 13:619. doi:10.1186/1471-2164-13-619. [PubMed: 23151021]
40. Fernandez SV, Robertson FM, Pei J, Aburto-Chumpitaz L, Mu Z, Chu K, Alpaugh RK, Huang Y, Cao Y, Ye Z, Cai KQ, Boley KM, Klein-Szanto AJ, Devarajan K, Addya S, Cristofanilli M. Inflammatory breast cancer (IBC): clues for targeted therapies. Breast cancer research and treatment. 2013; 140(1):23–33. doi:10.1007/s10549-013-2600-4. [PubMed: 23784380]

41. Ono Y, Abe K, Hayashi M, Chernov MF, Okada Y, Sakai S, Takakura K. Optimal visualization of multiple brain metastases for gamma knife radiosurgery. Acta neurochirurgica Supplement. 2013; 116:159–166. doi:10.1007/978-3-7091-1376-9_25. [PubMed: 23417475]

42. Bruzzone MG, D'Incerti L, Farina LL, Cuccarini V, Finocchiaro G. CT and MRI of brain tumors. The quarterly journal of nuclear medicine and molecular imaging : official publication of the Italian Association of Nuclear Medicine. 2012; 56(2):112–137.

43. Price SJ. Advances in imaging low-grade gliomas. Advances and technical standards in neurosurgery. 2010; 35:1–34. [PubMed: 20102109]

44. Perilongo G, Garre ML, Giangaspero F. Low-grade gliomas and leptomeningeal dissemination: a poorly understood phenomenon. Child's nervous system : ChNS : official journal of the International Society for Pediatric Neurosurgery. 2003; 19(4):197–203. doi:10.1007/s00381-003-0733-1.

45. Lee EK, Lee EJ, Kim MS, Park HJ, Park NH, Park S 2nd, Lee YS. Intracranial metastases: spectrum of MR imaging findings. Acta radiologica. 2012; 53(10):1173–1185. doi:10.1258/ar.2012.120291. [PubMed: 23081958]

46. Murrell DH, Hamilton AM, Mallett CL, van Gorkum R, Chambers AF, Foster PJ. Understanding Heterogeneity and Permeability of Brain Metastases in Murine Models of HER2- Positive Breast Cancer Through Magnetic Resonance Imaging: Implications for Detection and Therapy. Translational oncology. 2015; 8(3):176–184. doi:10.1016/j.tranon.2015.03.009. [PubMed: 26055175]

47. Perera M, Ribot EJ, Percy DB, McFadden C, Simedrea C, Palmieri D, Chambers AF, Foster PJ. In Vivo Magnetic Resonance Imaging for Investigating the Development and Distribution of Experimental Brain Metastases due to Breast Cancer. Translational oncology. 2012; 5(3):217–225. [PubMed: 22741041]

48. Murrell DH, Foster PJ, Chambers AF. Brain metastases from breast cancer: lessons from experimental magnetic resonance imaging studies and clinical implications. Journal of molecular medicine. 2013 doi:10.1007/s00109-013-1108-z.

49. Heyn C, Ronald JA, Ramadan SS, Snir JA, Barry AM, MacKenzie LT, Mikulis DJ, Palmieri D, Bronder JL, Steeg PS, Yoneda T, MacDonald IC, Chambers AF, Rutt BK, Foster PJ. In vivo MRI of cancer cell fate at the single-cell level in a mouse model of breast cancer metastasis to the brain. Magnetic resonance in medicine : official journal of the Society of Magnetic Resonance in Medicine / Society of Magnetic Resonance in Medicine. 2006; 56(5):1001–1010. doi:10.1002/mrm.21029.

50. Greig NH, Genka S, Daly EM, Sweeney DJ, Rapoport SI. Physicochemical and pharmacokinetic parameters of seven lipophilic chlorambucil esters designed for brain penetration. Cancer chemotherapy and pharmacology. 1990; 25(5):311–319. [PubMed: 2306790]

51. Adkins CE, Nounou MI, Hye T, Mohammad AS, Terrell-Hall T, Mohan NK, Eldon MA, Hoch U, Lockman PR. NKTR-102 Efficacy versus irinotecan in a mouse model of brain metastases of breast cancer. BMC cancer. 2015; 15:685. doi:10.1186/s12885-015-1672-4. [PubMed: 26463521]

52. Nduom EK, Yang C, Merrill MJ, Zhuang Z, Lonser RR. Characterization of the blood- brain barrier of metastatic and primary malignant neoplasms. Journal of neurosurgery. 2013 doi:10.3171/2013.3.JNS122226.

53. Bulnes S, Argandona EG, Bengoetxea H, Leis O, Ortuzar N, Lafuente JV. The role of eNOS in vascular permeability in ENU-induced gliomas. Acta neurochirurgica Supplement. 2010; 106:277–282. doi:10.1007/978-3-211-98811-4_52. [PubMed: 19812964]

54. Chaitanya GV, Cromer WE, Wells SR, Jennings MH, Couraud PO, Romero IA, Weksler B, Erdreich-Epstein A, Mathis JM, Minagar A, Alexander JS. Gliovascular and cytokine interactions modulate brain endothelial barrier in vitro. Journal of neuroinflammation. 2011; 8:162. doi:10.1186/1742-2094-8-162. [PubMed: 22112345]

55. Argyriou AA, Giannopoulou E, Kalofonos HP. Angiogenesis and anti-angiogenic molecularly targeted therapies in malignant gliomas. Oncology. 2009; 77(1):1–11. doi:10.1159/000218165. [PubMed: 19439998]

56. Castejon OJ. Ultrastructural pathology of endothelial tight junctions in human brain oedema. Folia neuropathologica / Association of Polish Neuropathologists and Medical Research Centre, Polish Academy of Sciences. 2012; 50(2):118–129.

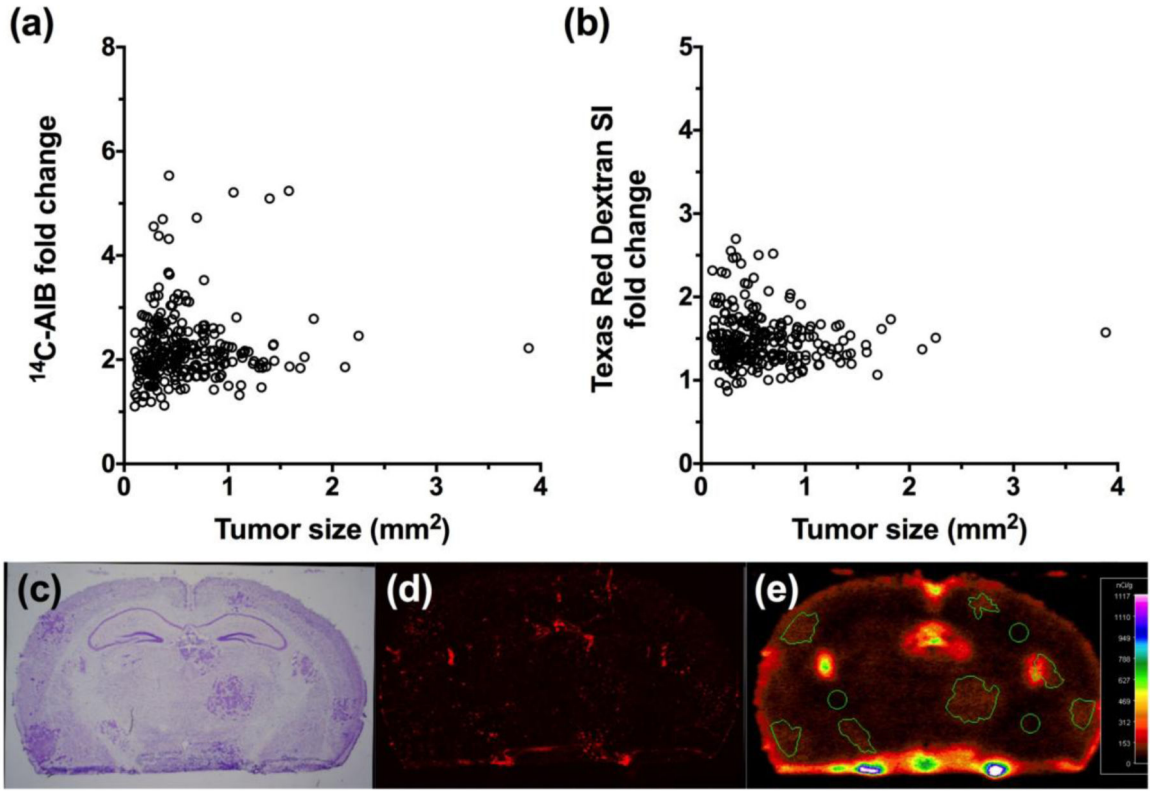

Figure 1. Passive permeability changes in brain metastases in the 4T1-BR5 model

The relative ^{14}C-AIB permeability fold-change in relation to metastasis size (mm^2) revealed little correlation (r^2=0.23) (a). The permeability fold-change of Texas Red dextran compared to metastasis size (mm^2) did not correlate (r^2=0.069) (b). A representative brain slice (approximately 0.86mm rostral to Bregma) bearing 4T1-BR5 metastases (c; cresyl violet) and its corresponding TRD fluorescence (d) and ^{14}C-AIB autoradiograph (e).

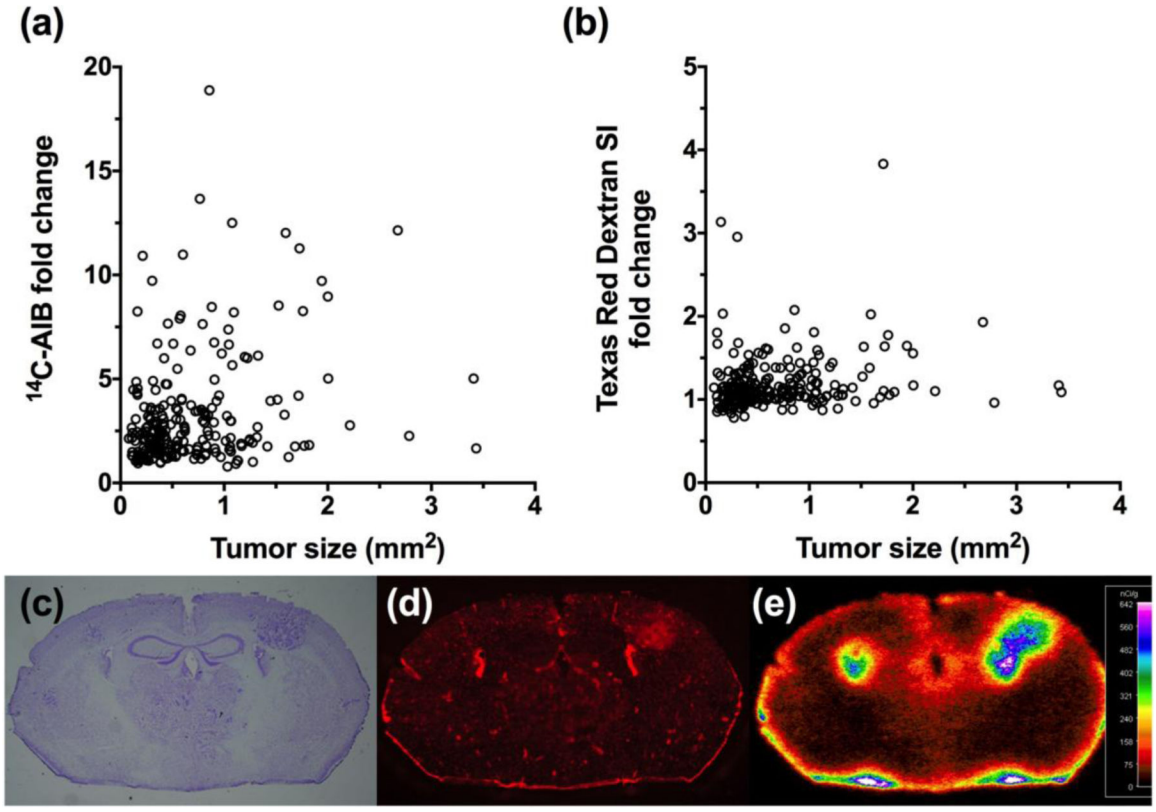

Figure 2. Passive permeability changes in brain metastases in the JIMT-1-BR3 line

The relative ^{14}C-AIB permeability fold-change in relation to metastasis size (mm^2) revealed no correlation (r^2=0.0038) (a). The permeability fold-change of Texas Red dextran compared to metastasis size (mm^2) did not correlate (r^2=0.0072) (b). A representative brain slice (approximately 1.7mm caudal to Bregma) bearing JIMT-1-BR3 metastases (c; cresyl violet) and its corresponding TRD fluorescence (d) and ^{14}C-AIB autoradiograph (e).

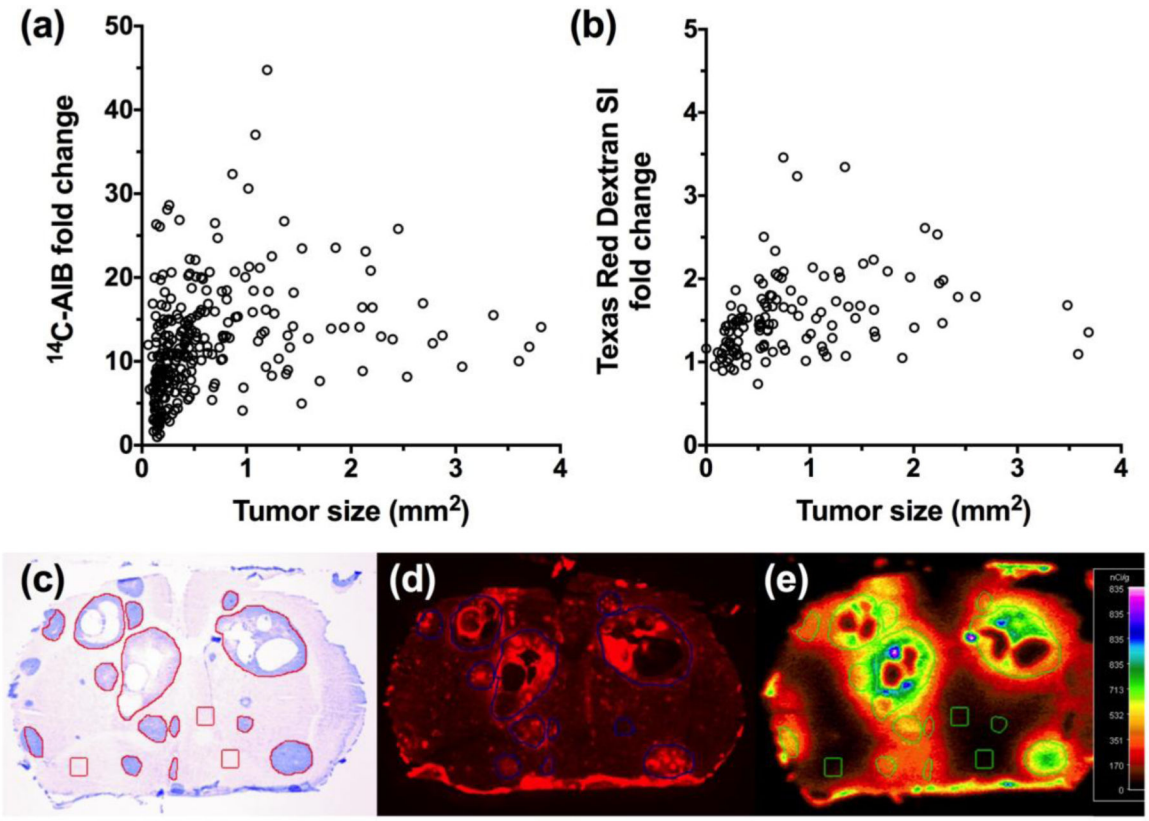

Figure 3. Passive permeability changes in brain metastases in the MDA-MB-231BR-HER2+ line

The relative ^{14}C-AIB permeability fold-change in relation to metastasis size (mm^2) revealed no correlation (r^2=0.032) (a). The permeability fold-change of Texas Red dextran compared to metastasis size (mm^2) did not correlate (r^2=0.062) (b). A fluorescence image of a representative brain slice (approximately 2.0mm caudal to Bregma) bearing MDA-MB-231BR-HER2+ metastases expressing eGFP (c) and its corresponding TRD fluorescence (d) and ^{14}C-AIB autoradiograph (e).

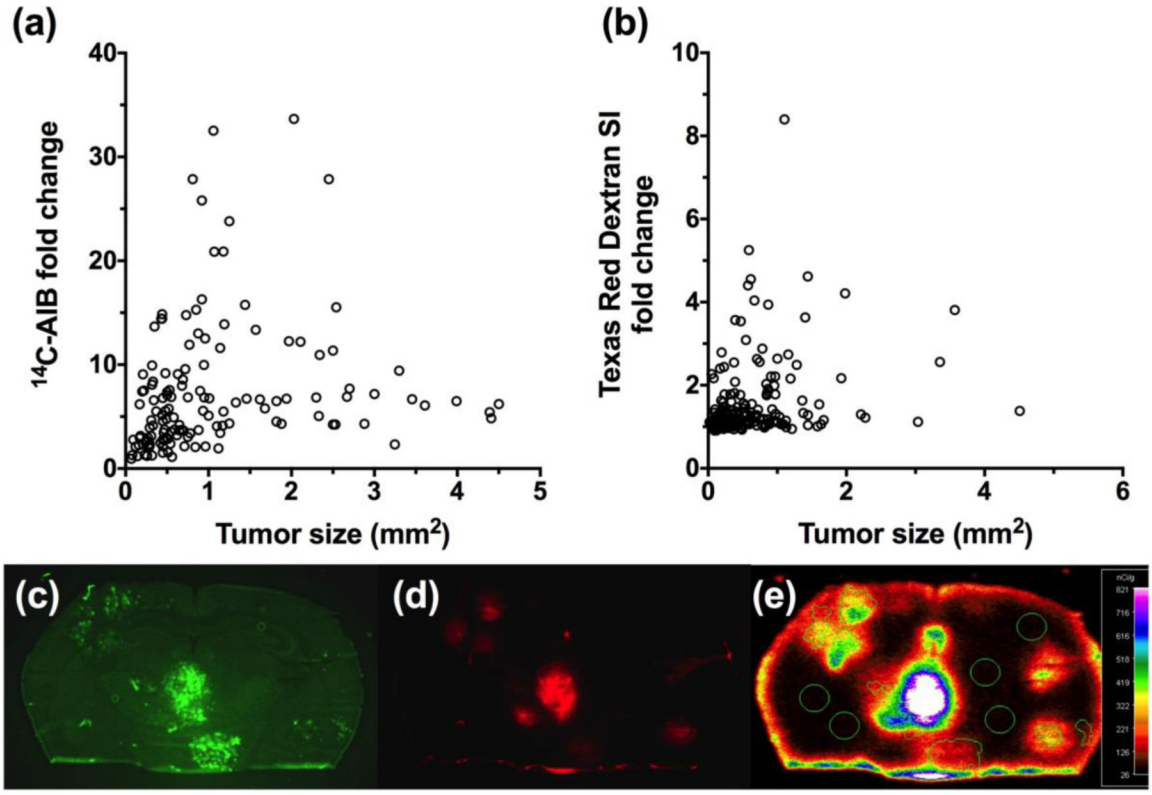

Figure 4. Passive permeability changes in brain metastases in the MDA-MB-231BR line

The relative ^{14}C-AIB permeability fold-change in relation to metastasis size (mm^2) revealed no correlation (r^2=0.077) (a). The permeability fold-change of Texas Red dextran compared to metastasis size (mm^2) did not correlate (r^2=0.031) (b). A representative brain slice (approximately 2.0mm caudal to Bregma) bearing 231BR metastases (c; cresyl violet) and its corresponding TRD fluorescence (d) and ^{14}C-AIB autoradiograph (e).

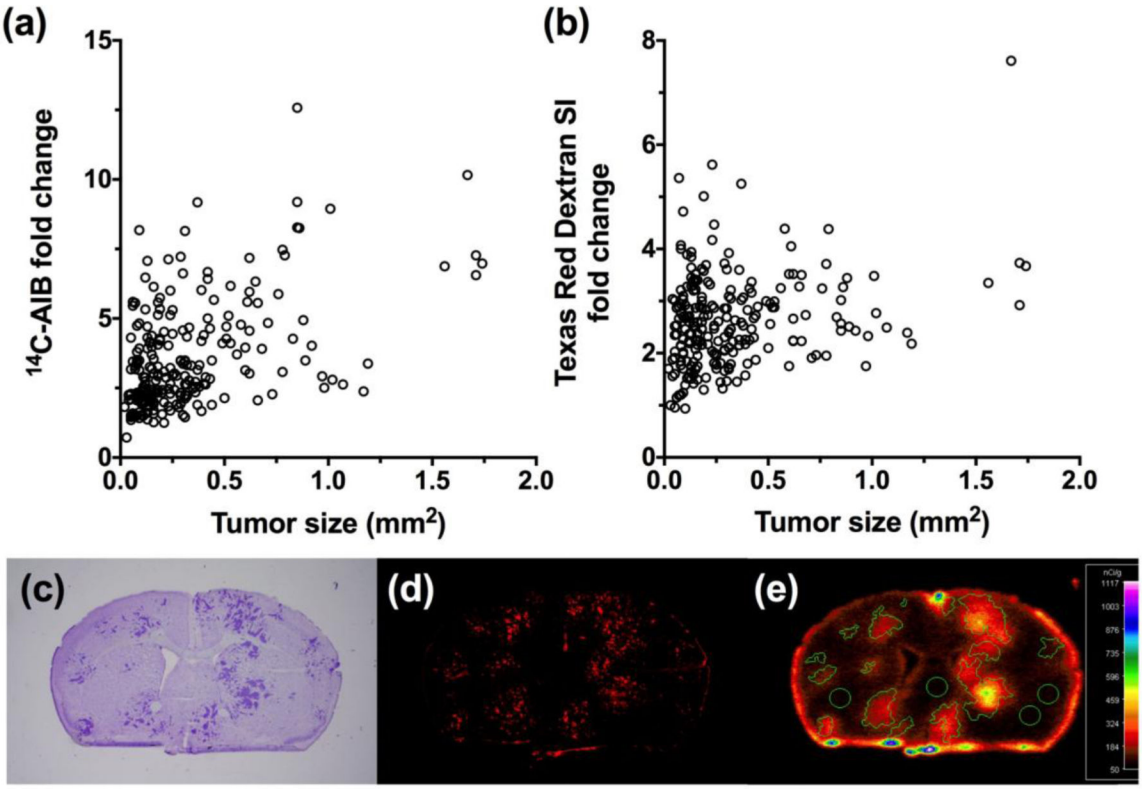

Figure 5. Passive permeability changes in brain metastases in the SUM190-BR3 line

The relative ^{14}C-AIB permeability fold-change in relation to metastasis size (mm^2) revealed little correlation (r^2=0.210) (a). The permeability fold-change of Texas Red dextran compared to metastasis size (mm^2) did not correlate (r^2=0.008) (b). A representative brain slice (approximately 0.35mm rostral to Bregma) bearing SUM190-BR3 metastases (c; cresyl violet) and its corresponding Texas Red dextran fluorescence (d) and ^{14}C-AIB autoradiograph (e).

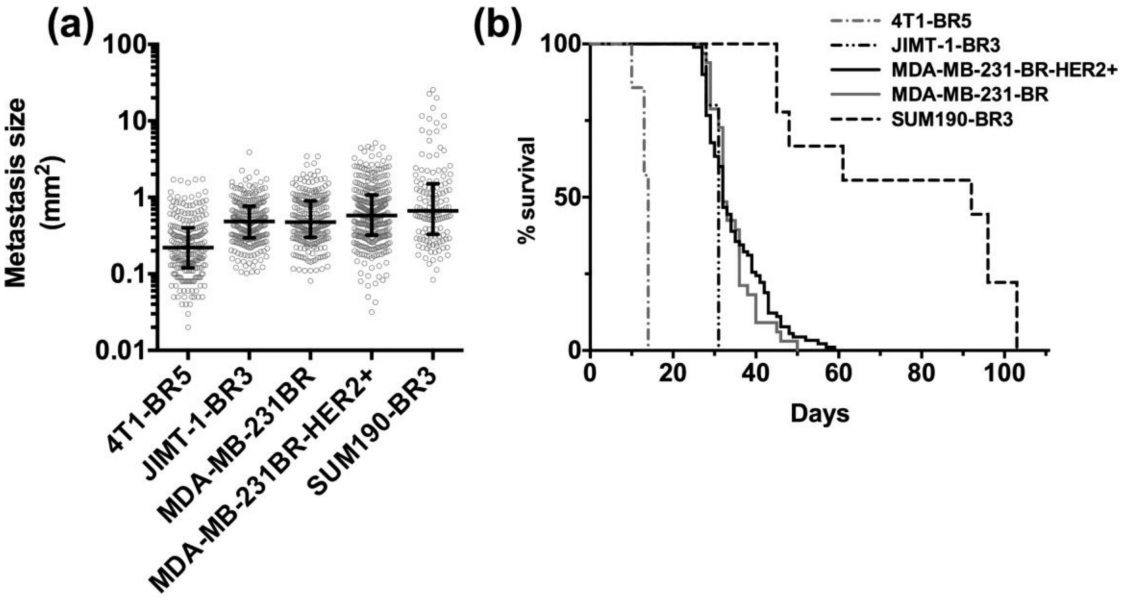

Figure 6. Metastases size and survival in preclinical brain metastases of breast cancer

The metastasis size and survival among five preclinical models of brain metastases of breast cancer. The median brain metastasis size (mm^2) and interquartile ranges (IQR) in each preclinical model (a). Each scatter point in panel (a) represents a single metastasis. The size of metastases in the 4T1-BR5 model was different ($p<0.001$) from all other models and the SUM190-BR3 model was also different ($p<0.005$) from all models except the MDA-MB-231BR-HER2+ ($p>0.05$). Additionally, JIMT-1-BR3 was different ($p<0.05$) from MDA-MB-231BR-HER2+ but not MDA-MB-231BR ($p>0.05$). The Kaplan-Meier survival plot of each experimental metastatic breast cancer model (b) (ANOVA; Dunn's multiple comparison test, *$p<0.005$ **$p<0.001$).

Table 1

Metastases permeability to ^{14}C-AIB and TRD and the correlation of each to lesion size for each model of brain metastases.

			AIB permeability (fold increase)		*AIB permeability vs. size (mm2)*	TRD permeability (fold increase)		*TRD permeability vs. size (mm2)*
Cell Line	***N (mice)***	***N (metastases)***	***median***	***IQR***	r^2	***median***	***IQR***	r^2
4T1-BR5	4	229	3.02	2.23 - 4.49	0.230	2.53	2.02 - 3.08	0.069
JIMT-1-BR3	5	256	2.08	1.83 - 2.47	0.004	1.43	1.28 - 1.62	0.007
MDA-MB-231BR-HER2+	5	184	5.51	3.09 - 8.82	0.032	1.18	1.06 - 1.58	0.062
MDA-MB-231BR	6	233	2.31	1.61 - 3.60	0.077	1.10	1.01 - 1.24	0.031
SUM190-BR3	5	285	11.90	7.73 - 16.28	0.210	1.43	1.18 - 1.73	0.008

The number of mice used in each preclinical model and the number of brain metastases analyzed are listed. Median metastases permeability to ^{14}C-aminoisobutyric acid (AIB) or Texas Red dextran (TRD) for each model are shown in addition to interquartile ranges (IQR). The correlation of AIB and TRD to lesion size is reported (r^2) for each model of metastases.